

# Density Power Spectrum in Turbulent Thermally Bi-stable Flows

Adriana Gazol<sup>1</sup>

*Centro de Radioastronomía y Astrofísica, UNAM, A. P. 3-72, c.p. 58089, Morelia, Michoacán, México*  
a.gazol@crya.unam.mx

and

Jongsoo Kim<sup>2</sup>

*Korea Astronomy and Space Science Institute, 61-1, Hwaam-Dong, Yuseong-Ku, Daejeon 305-348, Korea*  
jskim@kasi.re.kr

## ABSTRACT

In this paper we numerically study the behavior of the density power spectrum in turbulent thermally bistable flows. We analyze a set of five three-dimensional simulations where turbulence is randomly driven in Fourier space at a fixed wave-number and with different Mach numbers  $M$  (with respect to the warm medium) ranging from 0.2 to 4.5. The density power spectrum becomes shallower as  $M$  increases and the same is true for the column density power spectrum. This trend is interpreted as a consequence of the simultaneous turbulent compressions, thermal instability generated density fluctuations, and the weakening of thermal pressure force in diffuse gas. This behavior is consistent with the fact that observationally determined spectra exhibit different slopes in different regions. The values of the spectral indexes resulting from our simulations are consistent with observational values. We do also explore the behavior of the velocity power spectrum, which becomes steeper as  $M$  increases. The spectral index goes from a value much shallower than the Kolmogorov one for  $M = 0.2$  to a value steeper than the Kolmogorov one for  $M = 4.5$ .

*Subject headings:* hydrodynamics — instabilities — ISM: structure — methods: numerical — turbulence

## 1. Introduction

The turbulent nature of the interstellar medium (ISM) is believed to play a crucial role on the determination of its density and velocity structure (see Elmegreen & Scalo 2004; Scalo & Elmegreen 2004; and Mac Low & Klessen 2004, for recent reviews). A useful characterization of the properties of a random density or velocity distribution is given by the spatial power spectrum. This function can be measured for different components of the interstellar gas by using different observational techniques. In the warm ionized medium (WIM) interstellar scintillation (ISS) measurements have lead to a Kolmogorov slope density power spec-

trum, which is valid for scales expanding over  $\approx 5$  orders of magnitude from  $10^{8.3}$  to  $10^{15}$  cm (e.g. Armstrong, Rickett & Spangler 1995). The same authors found that when ISS data are combined with measurements of differential Faraday rotation angle and electron density gradients, constraints can be put on the spectrum at much larger scales, suggesting an extension of the precedent result to scales of  $\approx 10^{20}$  cm.

For the atomic gas, the 21cm hydrogen line provides a variety of useful tools to measure statistical properties of turbulence. In particular, some estimates of the spatial power spectrum for the HI 21cm emission distribution in the Galactic Disk show a power law behavior with different slopes.

From individual channel maps, Crovisier & Dickey (1983), reported a value of  $-3^1$  while Green (1993) found a range from -3 to -2.2. For the Small Magellanic Cloud (SMC) Stanimirović et al. (1999) also report a power law behavior with an averaged slope of  $-3.04 \pm 0.02$ , for the whole galaxy and an averaged slope of  $-2.85 \pm 0.02$  for the eastern Wing. A similar behavior has been reported by Elmegreen, Kim & Staveley-Smith (2001) for the HI integrated emission of the central region of the Large Magellanic Cloud. The same authors found a change in the spectrum slope, flattening from -3.66 to -2.66, at  $\approx 100$ pc and interpreted it as the consequence of scales in the plane of the sky becoming larger than the depth of the medium. In that case a two dimensional medium would be described at scales larger than  $\approx 100$ pc. A recent study of the HI intensity fluctuations power spectrum of six dwarf galaxies (Dutta et al. 2009) reports shallower power law behaviors with slopes of  $\approx -1.5$  for one group of galaxies and  $\approx -2.6$  for another. They interpret the shallower spectrum of the first group as possibly due to the presence of two-dimensional (2D) turbulence.

The observed spatial power spectrum contains information about both, the three-dimensional (3D) density distribution and the 3D velocity field, and its inversion to a unique 3D density or velocity power spectra is not easy. A method to relate the fluctuations of intensity in position-position-velocity data cubes by changing the thickness of the velocity slice has been proposed by Lazarian & Pogosyan (2000). This method, called Velocity Channel Analysis (VCA), has been numerically proved for high resolution isothermal simulations by (Padoan et al. 2006) and applied in statistical studies of galactic and extragalactic atomic gas. Stanimirović & Lazarian (2001) analyzed the spectrum of the observed intensity fluctuations as a function of the velocity slice thickness in the SMC and obtain spectral indices of -3.3 and -3.4 for the 3D density and the 3D velocity spectra, respectively. For the Milky Way, two regions in the fourth Galactic quadrant have been studied by Dickey et al. (2001) using the same method. They find that for a high latitude region the slope of the 3D density spectrum is -4 with an apparently lit-

tle effect of velocity fluctuations, whereas for a low latitude region, the slope of the density spectrum can not be deduced from their data, which are consistent with a velocity distribution having a structure function with a slope of 0.2. Other method to disentangle the statistical properties of the three dimensional cold HI density distribution at small scales in the Perseus arm towards Cas A and in the outer and local arms towards Cygnus A has been used by Deshpande et al. (2000). They predict the power-law index of the density spectrum based on that of the observed optical depth, and obtain a slope of -2.75 for the two first cases, while for the local arm towards Cygnus A, they obtain -2.5. Miville-Deschênes et al. (2003) presented interferometric 21 cm observations of Ursa Major high cirrus and used the spectra of the integrated emission and of the centroid velocity fields to deduce the three-dimensional spectral index of the density and velocity fields at scales of  $\approx 5$ pc, and found a value of -3.6 for both. In the context of molecular clouds other methods to measure the density power spectrum have been developed (see e.g. Bensch et al. 2001), and find values in the same range as those obtained for the HI gas. For instance, Stutzki et al. (1998) find -2.8 for the Polaris Flare.

The interstellar density power spectrum has also been numerically studied. The case of compressible isothermal flows has been addressed by Kim & Ryu (2005), who found that the slope of the density power spectrum becomes gradually shallower as the rms Mach number ( $M_{\text{rms}}$ ) increases, going from a Kolmogorov slope for transonic turbulence, to -0.52 for  $M_{\text{rms}} = 12$  (note that this slope corresponds to the spectrum integrated over the angles, in this case, the Kolmogorov slope is -5/3 instead of -11/3). They propose that this behavior reflects the development of sheetlike and filamentary structures for large values of  $M_{\text{rms}}$  and provides a possible explanation for the fact that for the WIM the density power spectrum shows a Kolmogorov slope while the corresponding slope for the HI tends to be shallower. Recently, Federath et al. (2009) numerically studied the density statistics of high Mach number isothermal simulations with two different kinds of forcing, finding that for the same Mach number compressive driving leads to a significantly steeper power spectrum than the one obtained with solenoidal forcing.

<sup>1</sup>Note that this is an average value and that the slopes of individual channels vary from  $\approx -2$  to  $\approx -4$

In an attempt to understand available observations, Hodge & Deshpande (2006) presented a simplified model in which the complex distribution of atomic hydrogen is determined only by the superposition of voids generated by supernovae, either with or without kinematical effects. They obtain a velocity spectrum with a power law behavior close to the Kolmogorov spectrum and a (column) density spectrum with a slope of -3.4 for the nonkinematical case. For their kinematical case the density power spectrum does not develop a range with a power law behavior.

The case of density fluctuations from magnetized isothermal turbulence has been recently studied in detail by Kowal et al. (2007) whose results for the power spectrum show that for subsonic turbulence, the slope presents slight changes with the sonic Mach number, while when motions become supersonic, the presence of pronounced small scale structure produces a flattening of the spectra, as in the non magnetized case (Kim & Ryu 2005). This behavior is observed for superalfvénic as well as for subalfvénic simulations.

The HI density distribution is however strongly influenced by the presence of the isobaric mode of thermal instability (TI, Field 1965) and the interplay between this instability and turbulence has important consequences on the formation of atomic as well as molecular interstellar structure (e.g. Hennebelle et al. 2009). The density spectrum for cooling thermally bistable turbulent gas has been presented by Hennebelle & Audit (2007), who found a -0.4 slope for the integrated spectrum.

However, the behavior of the density power spectrum of thermally unstable gas in different turbulent conditions and in particular its behavior for distinct values of the sonic Mach number, has not been addressed. Although the driving mechanisms for interstellar turbulence remain a matter of debate (Mac Low & Klessen 2004; Brunt et al. 2009; Federrath et al. 2010), recent observational results (Tamburro et al. 2009) using a sample of galaxies from the HI Nearby Galaxy Survey show that all the studied galaxies exhibit a systematic radial decline in the HI line width which implies a radial decline in kinetic energy density of HI. Previous reports of the same behavior can be found, for example for NGC1058 (Petric & Rupen 2007), NGC5474 (Rownd et al. 1994), or NGC6946 (Boulanger & Viallefond 1992).

In this work we present a numerical study of the density power spectrum for cooling turbulent gas in physical conditions similar to those in the interstellar atomic gas. The outline of the paper is the following. In §2 we describe the model, in §3 we present results concerning the effects of varying the sonic Mach number on the density and velocity power spectra. For the former we study the whole gas distribution as well as the behavior of gas at specific temperature intervals. Then, in §4 we discuss these results in the context of previous work and finally in §5 we give a summary and some conclusions.

## 2. The model

We solve the hydrodynamic equations in three dimensions to simulate a cubic region of 100 pc on a side with periodic boundary conditions. The equations are solved using a total variation diminishing scheme with a linearized Riemann solver (Roe 1981; Harten 1983; Kim et al. 1999). The energy equation includes a constant background heating rate and a radiative cooling function with a piece-wise power-law dependence on the temperature obtained by Sánchez-Salcedo et al. (2002) as a fit of the standard  $P$  vs.  $\rho$  curve of Wolfire et al. (1995) at constant heating rate,  $\Gamma_0$ . In thermal equilibrium conditions this curve implies that the gas is thermally unstable under the isobaric mode for  $313 \text{ K} < T < 6102 \text{ K}$ , and marginally stable for  $141 \text{ K} < T < 313 \text{ K}$ . The corresponding thermal equilibrium densities are  $n = 0.60, 3.2$  and  $7.1 \text{ cm}^{-3}$ , for  $T = 6102, 313$  and  $141 \text{ K}$ , respectively. For the fit, the assumed value of the heating rate is  $\Gamma_0 = 2.51 \times 10^{-26} \text{ ergs}^{-1} \text{ H}^{-1}$  (where  $\text{H}^{-1}$  means per hydrogen atom mass).

The random turbulent forcing is done in Fourier space at a specified narrow wave-number band,  $1 \leq k \leq 2$ , where  $k \equiv \sqrt{k_x^2 + k_y^2 + k_z^2}$ . The turbulent driving is solenoidal, with the Gaussian deviates having zero mean and unitary standard deviation. The amplitude of velocity perturbations is fixed by a constant injection rate of kinetic energy as in the prescription of Mac Low (1999), with the difference that we use a distinct random seed at each driving time. The kinetic energy input rate is chosen as to approximately maintain a desired rms sonic Mach number  $M$ , which is expressed with respect to the sound speed at  $10^4 \text{ K}$ ,  $c_s = 9.1$

km s<sup>-1</sup>. Note that dividing the box size by  $c_s$ , we find a time unit of  $t_0 = 10.8$  Myr.

In all the simulations presented in §3, the fluid is initially at the rest, the density and the temperature are uniform and have thermally unstable values ( $n_0 = 1$  cm<sup>-3</sup>,  $T_0 = 2399$  K).

### 3. Results

In this section we present results from one set of five simulations with 512<sup>3</sup> grid points and five different values of  $M$  namely 0.2, 0.6, 1.3, 4.0, and 4.5 (i.e from 0.41, 1.22, 2.65, 8.16, and 9.2 when computed with respect to the sound speed at the initial temperature).

In Figure 1 (*left column*) we show two dimensional cuts of the density field for each simulation. All the images have been done with the same color scale. As expected, lower  $M$  simulations show a smaller density contrast and sharper boundaries between dense regions and its surroundings, due to the relatively undisturbed development of TI. The later behavior is better appreciated in Figure 2, where different color scales have been used and where contours at temperatures delimiting the thermally unstable regime have been placed. In this figure it also can be seen that for low  $M$  simulations, thermally unstable gas does just exist at the boundaries between gas at the two thermally stable regimes.

#### 3.1. Notation

We denote by  $P_a(k)$  the integrated power spectrum, i.e., the integral over spherical shells with radius  $k = |\mathbf{k}|$  of the squared Fourier transform of the physical quantity  $a$  and for simplicity, we refer to  $P_a(k)$  as the “Power Spectrum”. As usual,  $\mathbf{k} = (k_x, k_y, k_z)$  is the wave-vector. This convention is frequently used (e.g. Kim & Ryu 2005, Kitsionas et al. 2009) but is not universal, sometimes (e.g. Hennebelle & Audit 2007) the power spectrum is defined by the quantity  $p_a(k) \propto k^{1-D} P_a(k)$ , where  $D$  is the dimension of the distribution, which is the non integrated power spectrum. For reference, for Kolmogorov turbulence  $p_v(k) \propto k^{-11/3}$  whereas  $P_v(k) \propto k^{-5/3}$ .

All the power spectra presented bellow are temporally averaged results. The time intervals used for each simulation are listed in Table 1 in units of the corresponding turbulent crossing time  $t_{\text{turb}}$ .

We define  $t_{\text{turb}} = l_{\text{for}}/(Mc_s)$  with  $l_{\text{for}} = 50$  pc being the characteristic scale of the turbulent forcing. In this table we also present the final time reached by each simulation and the number of snapshots we use to compute the average. In Figure 3 we present the Mach number as a function of time for the five simulations presented in next two sections. The x-axis has  $t_0$  units in order to emphasize that, in these units, much longer integration times have been used for lower values of  $M$ . In  $t_0$  units, the lower limit of the time interval used for averaging power spectra (i.e. the lower limit in the third column of Table 1) corresponds to 10.0, 5.0, 2.3, 1.0, and 1.0 for  $M$  equal to 0.2, 0.6, 1.3, 4.0, and 4.5, respectively. It can thus be seen from the figure that the power spectra have been averaged in a stationary regime.

#### 3.2. Density and Velocity Spectra for the whole simulation

Time averaged density power spectra  $P_\rho$ , are shown in Figure 4 along with power law least-squares fits computed for  $4 \leq k \leq 14$ , which implies physical scales ranging from  $\approx 7$  pc to 25 pc. The power law indexes obtained from those fits for each simulation are listed in Table 2 along with power law indexes resulting from similar fits for all the power spectra discussed in the present paper. As in the isothermal case reported by Kim & Ryu (2005), the absolute value of the slope (in logarithmic coordinates) decreases as the value of  $M$  increases. For our simulations it goes from  $-0.84$  for  $M = 0.15$  to  $-0.10$  for  $M = 4.5$ . These values are consistent with the value previously reported by Hennebelle & Audit (2007). We have also computed column density power spectra  $P_\Sigma$ , by projecting the 3D density field on the  $z$  direction and using the resulting 2d distribution. As expected, due to the reduced amount of points, these spectra (displayed in Figure 5) develop more fluctuations than those obtained from the full three dimensional distribution. The best power law fits of these spectra, whose slopes are listed in Table 2, show that they are steeper than spectra obtained from the full 3D distribution and have a similar trend as them, namely that they become flatter as  $M$  is increased, with values ranging from  $-1.64$  for  $M = 0.2$  to  $-1.11$  for  $M = 4.0$ . Note however that the slope of the column density power spectrum for  $M = 4.5$  is larger than the one for  $M = 4.0$ . As

expected, the power-law region of  $k^{-1}P_\Sigma$  behaves in approximately the same way as the power-law region of  $k^{-2}P_\rho$  implying that  $p_\Sigma$  and  $p_\rho$  have approximately the same spectral index as predicted by Stutzki et al. (1998) and shown by Brunt et al. (2010). This fact has previously been numerically confirmed by Mac Low & Ossenkopf (2000) and Federrath et al. (2009). For all the spectra in Figure 5 it can also be seen a change of sign in slope at high frequencies. This change, that does not occur for  $P_\rho$ , is due to the presence of small three dimensional structures that do not overlap when projection is done (see Figure 1, *right column*).

It is also interesting to study the behavior of the velocity power spectrum  $P_v$  as  $M$  changes (see Fig. 6), which shows significant variations when the Mach number changes. In particular, the slope resulting from a power-law fit at the same wave number range as in the density spectra case, goes from -1.79 (steeper than the Kolmogorov slope of -5/3) for  $M = 4.5$  to -1.08 for  $M = 0.2$ . This behavior is different from the one reported by Kim & Ryu (2005), for the one dimensional case, where the slope was nearly equal -2 irrespective of the rms Mach number. A similar slope has been reported by Kritsuk et al. (2007) for highly compressible isothermal turbulence. Recently, for an isothermal gas with  $M = 5.5$  Federrath et al. (2009) found slopes of  $-1.86 \pm 0.05$  and  $-1.94 \pm 0.05$  for solenoidal and compressive forcing, respectively; whereas Schmidt et al. (2009) obtained a value of -1.9 for  $M = 2.5$ , also in the isothermal case. For two-dimensional non isothermal gas with  $M \approx 1$ , Hennebelle & Audit (2007) obtain a velocity spectrum in good agreement with the Komogorov law.

As stated by Kitsionas et al. (2009) the density weighted spectrum represents an appropriate statistical tool to study compressible turbulence because it takes into account the fact that in the compressible case most of the mass ends up in small volumes. This spectrum however can be computed as the power spectrum of the quantity  $\rho^{1/2}\mathbf{v}$  which is directly related to the kinetic energy, or as the power spectrum of  $\rho^{1/3}\mathbf{v}$ , that arises from the condition of constant mean volume energy transfer rate, which is valid for a compressible fluid in a steady state (Lighthill 1955, see also Kritsuk et al. 2007). Here we show both. In Figure 7a the power spectrum of  $\sqrt{\rho}\mathbf{v}$  is shown. As expected due to the increased density power at

small scales, these spectra are notoriously flatter than  $P_v$  with power-law fit slopes ranging from -0.77 to -0.85. Moreover, in this case the slope value range is narrower than for the density and the velocity cases and do not show any systematic behavior when varying  $M$ . The slopes we get are comparable to the value reported by Hennebelle & Audit (2007) for two dimensional simulations. On the other hand,  $P_{\rho^{1/3}\mathbf{v}}$  (Fig. 7b), is steeper than  $P_{\rho^{1/2}\mathbf{v}}$ , and except for the lower value of  $M$  follows the same trend as the velocity spectrum, i.e. it steepens as  $M$  decreases. The last fact can be understood as a consequence of the lower dependence on  $\rho$ . Also, the slope value range is larger for  $P_{\rho^{1/3}\mathbf{v}}$  but is still narrower than for the density and the velocity spectra. This implies that for our simulations the quantity  $\rho^{1/2}v$  has more well defined scaling law than the quantity  $\rho^{1/3}v$ .

### 3.3. Density Spectra for Different Temperature Ranges

The pure development of the isothermal mode of thermal instability (TI) in the atomic galactic gas allows to distinguish three thermodynamic regimes: stable warm gas, unstable gas, and stable cold gas. Figure 8 shows the density power spectra we obtain for each of these regimes. The temperature limits we use to separate the gas are arbitrarily chosen as those determined by the cooling function, i.e. 313 K and 6110 K, implying that our warm, unstable and cold gases have temperatures,  $T > 6110\text{K}$ ,  $313\text{K} < T < 6110\text{K}$ , and  $T < 313\text{K}$ , respectively. As a first approximation we compute each spectrum by considering only those grid points where the temperature lies in the desired range and assigning a zero value elsewhere. We are aware that this procedure can introduce high frequency noise in the spectrum but this effect should affect in a comparable way all the spectra in a given temperature range. Also we recall that the slopes are measured for relatively small values of  $k$  (see §3.2), which is hardly affected by the high frequency noise.

The density power spectrum for the warm gas  $P_{w\rho}$ , the unstable gas  $P_{u\rho}$  and the cold gas  $P_{c\rho}$  follows the same behavior as  $P_\rho$ , namely it becomes flatter as  $M$  increases (see Table 2). When comparing the slopes obtained for spectra at different temperature regimes for the same value of  $M$ , the sole consistent behavior is that at large  $M$

(transonic or supersonic with respect to the gas at  $10^4\text{K}$ ) the spectrum flattens as the temperature decreases, and for  $M = 4.0$  and  $4.5$  the slope even changes its sign. As the averaged turbulent velocity is approximately the same in all the three temperature ranges implying that colder gas has considerably larger Mach numbers, this behavior is not surprising because is the same as the one reported by Kim & Ryu (2005). The slopes are however much shallower than the ones they obtain. For instance, in our simulation with  $M = 1.3$  the slope of the power spectrum for cold gas is  $-0.12$ , whereas the slope of the power spectrum they get for an isothermal simulation with  $M = 7.3$  is  $-0.75$  (note that the Mach number for gas at  $313\text{K}$  corresponding to  $M = 1.3$  is  $7.35$ ).

### 3.4. A comparison with the isothermal case

In order to confirm that turbulence statistics is significantly affected by the presence of TI, in this section we compare a thermally unstable simulation with an isothermal one. We use our lower  $M$  simulation because in this case the velocity power spectrum for the isothermal regime is expected to have a slope close to that predicted by Kolmogorov (i.e.  $-5/3$ ). For completeness sake we do also include a comparison between density power spectra. In Figure 9 we show density (*left*) and velocity spectra (*right*) for the thermally unstable (*solid line*) and the isothermal (*dotted line*) simulations. For the former case the fitted slopes are the same as those reported in Table 2, while for the isothermal case slopes are  $-1.89$  and  $-1.60$  for the density and the velocity spectrum, respectively. The first value is consistent with the trend found by Kim & Ryu (2005) and the second one is close to the expected value. These slopes indicate that the effects presented in previous sections concerning the flattening of the density and the velocity power spectra in thermally unstable flows are not due to the time interval we use to compute averaged values and that the presence of TI has in fact important effects on turbulence statistics. Note that all the spectra in Figure 9 have been computed by averaging values in the same time interval (see Table 1) and that the isothermal simulation has been done with an isothermal version of the same code as the one described in §2.

## 4. Discussion

### 4.1. Relation with Previous Work

Observational results on the HI power spectrum show a power law behavior with an extended range of slope values. This is true for the spectrum resulting from intensity fluctuations as well as for the spectrum deduced for the underlying 3D density distribution. The latter spectrum describes the statistics of a density distribution strongly influenced by the presence of TI and turbulence. On the other hand, it is well known that TI can be triggered in the warm stable gas by turbulent motions characterized by large enough sonic Mach numbers (Hennebelle & Pérouault 1999) and that the density PDF is strongly influenced by the characteristics of turbulence (Klessen 2000; Federrath et al. 2008) as well as by the equation of state (e.g. Passot & Vázquez-Semadeni 1998, Nordlund & Padoan 1999, Li et al. 2003, Gazol et al. 2005, Kowal et al. 2007). In particular Passot & Vázquez-Semadeni (1998) showed that the density PDF is lognormal for isothermal flows ( $\gamma = 1$ , with  $\gamma$  being the effective polytropic index), but develops a power-law tail at high densities for  $\gamma < 1$ , and at low densities for  $\gamma > 1$ . For a polytropic self-gravitating gas Li et al. (2003) found imperfect lognormal distributions whose width increases as  $\gamma$  increases. The case of thermally unstable gas interacting with turbulent motions have been studied by Gazol et al. (2005). Using the same cooling function as the one used for the present work, they found bimodal distributions that become broader as  $M$  or the forcing scale increases. The bimodal character of the distributions is less pronounced for small forcing scales and for large values of  $M$ . On the other hand, different turbulent conditions have been suggested by the observational estimation of the available kinetic energy in the atomic gas of nearby galaxies (Tamburro et al. 2009). In this context, the results we presented in the previous section suggest that different slopes in the observed HI density power spectra could be due to different turbulent conditions, in particular different Mach numbers. Different values of the Mach number have been used by Elmegreen et al. (2001) in fractal models aimed to fit HI data, including the power spectrum, of the Large Magellanic Cloud. They found that the large amplitude of the observed intensity variations cannot

be achieved by turbulence alone; phase transitions are required. In models presented by these authors however, both the Mach number and the HI scale height are simultaneously modified making it impossible to isolate the effect of varying  $M$ .

The flattening of the density power spectrum as  $M$  is increased is consistent with results reported by Kim & Ryu (2005) for the isothermal hydrodynamic case and by Kowal et al. (2007) for the isothermal MHD case. Our spectra are shallower than the ones they obtain but they are consistent with the value reported by Hennebelle & Audit (2007) for two dimensional thermally bistable simulations. These authors interpret the relatively flat density power spectrum as a consequence of the strong and stiff density fluctuations produced by the development of TI rather than by highly supersonic motions. Our numerical experiments consider the effect of both. We can understand our results in terms of the predictions of Sachiev & Woyczynski (1996) concerning the power spectrum of density resulting from a velocity field governed by the Burgers equation in the presence of pressure forces. They find that in the limit of a negligible pressure force  $P_\rho$  does not depend on  $k$ , while in the presence of a pressure force  $P_\rho \propto k^{-2}$ . The effect of varying the turbulent conditions on the thermodynamic properties of a thermally bistable gas, has been studied by Gazol et al. (2005). For large scale forcing they found that as  $M$  increases, the local ratio of turbulent crossing time to cooling time decreases, causing transient structures in which the effective behavior is intermediate between the thermal-equilibrium and adiabatic regimes. In particular, the mean pressure in a given density interval drifts away from the thermal equilibrium value  $P_{\text{eq}}$  as  $M$  is increased, moving toward  $P > P_{\text{eq}}$  for the dense gas and toward  $P < P_{\text{eq}}$  for distributions centered at typical densities of the warm and the unstable gas. Flatter spectra in high  $M$  simulations could thus be produced by the weakening of pressure forces in diffuse gas. In the simulations presented here there are then three physical ingredients contributing to the flattening of the density power spectrum: density fluctuations produced by turbulence, density fluctuations produced by TI, and 'enhanced' density fluctuations produced by the interactions between turbulence and TI.

Direct comparison of the spectral indexes we

obtain for  $P_\rho$  with observations of the density power spectrum show that they only agree with values reported by Deshpande et al. (2000) and with those obtained by Dutta et al. (2009) for nearby dwarf galaxies. We recall that values in Table 2 should be multiplied by a factor  $k^{-2}$  in order to be comparable with observational data (see §3.1). Note that Dutta et al. (2009) find that, for all the galaxies in their sample, the power-law slope remains constant as the channel thickness is increased, suggesting that the fluctuations in the HI intensity are only due to density fluctuations, or that the slope of the velocity structure function is  $\approx 0$ .

Theoretical predictions by Lazarian and Pogosyan (2000) can be used to further compare our results with observational results, in particular with works reporting only spectral slopes from individual channel maps or averaged values over distinct velocity channels. The VCA method consists on gradually increase the velocity thickness of the sampling region until the slope of the observed two dimensional spectrum gets stabilized. For the thickest slices, the velocity information is averaged out and the power-law index of the three dimensional density spectrum  $n$  is recovered. For thin slices the method provides a relation between  $n$  and the three dimensional velocity spectral index. A slice is defined as "thin" if the turbulent velocity dispersion on the studied scale is smaller than the velocity slice thickness. Although this method have not been numerically tested for thermally bistable cases <sup>2</sup>, we can explore what we would get if we were observing our density distribution through a "thin" velocity slice (observing through a thick slice would give results on the second column of Table 2 plus -2). To do that, we need to combine slopes for  $P_\rho$  and slopes for  $P_v$  in the regime of a shallow three dimensional density ( $k^{-2}P_\rho \propto k^n$  with  $n > -3$ ) for a thin velocity slice (see Lazarian & Pogosyan, 2000). In this regime,  $n$  is related with the slope of the velocity structure function  $m$  (the three-dimensional velocity spectrum is then  $\propto k^{-3+m/2}$ ) through the index of the spatial power spectrum, which is proportional to  $k^{n+m/2}$ . In that case, for the hypothetically observed intensity spectrum  $P_{\text{obs}}$ ,

<sup>2</sup>Such a test is out of the scope of this work but we plan to present it elsewhere.

which combines information about density and velocity, we obtain slopes of -2.92, -2.76, -2.71, -2.93, and -2.89 for  $M = 0.2, 0.6, 1.3, 4$  and  $4.5$ , respectively. These values are in the range of values reported by Crovisier & Dickey (1983), Green (1993), Stanimirović et al. (1999), and Dutta et al. (2009). In this case the behavior of  $P_{\text{obs}}$  as the Mach number increases (i.e. a non systematic change) is consistent with the behavior we find for  $P_{\rho^{1/2}\mathbf{v}}$ , which is in turn consistent with the fact that  $P_\rho$  and  $P_{\mathbf{v}}$  show opposite trends. The behavior of  $P_{\text{obs}}$  as  $M$  increases, is in contrast inconsistent with the behavior of  $P_{\rho^{1/3}\mathbf{v}}$ , which tends to become shallower for lower Mach numbers. For our simulations, thus,  $P_{\rho^{1/2}\mathbf{v}}$  seems to be a more adequate quantity to take into account density and velocity contributions to the statistics. However, it should be noticed that similar slopes of  $P_{\rho^{1/2}\mathbf{v}}$ ,  $P_{\rho^{1/3}\mathbf{v}}$ , or  $P_{\text{obs}}$  could result from very different physical conditions. This implies that in order to relate power spectrum properties with physical conditions in the HI gas, and in particular with the Mach number, the distinction between density induced and velocity induced intensity fluctuations seems to be unavoidable. In cases where column density maps can be directly obtained, and the density power spectrum can be unambiguously measured the relationship between the density power spectrum and the Mach number can be easily established.

On the other hand, the behavior of the velocity spectrum, steepening as  $M$  increases, can be understood as follows. The fact that for larger values of  $M$  we get a slope larger than the Kolmogorov one, as other authors have done (e.g. Kritsuk et al. 2007; Schmidt et al. 2009; Federath et al. 2010) for the isothermal case is consistent with the effective polytropic index approaching 1 as  $M$  becomes larger (Gazol et al. 2005). In high  $M$  simulations turbulent motions generated by the development of TI, which are typically of the order of tenths of  $\text{km s}^{-1}$  (Kritsuk & Norman 2002; Piontek & Ostriker 2004), are much smaller than the forcing generated velocities. Instead, at small values of  $M$ , the modest amplitudes of turbulence produced by TI can considerably contribute to the gas velocity. Furthermore, the almost undisturbed development of TI in small  $M$  simulations occurs only at relatively small scales ( $\lesssim 10\text{pc}$ , see Heitsch et al. (2008) for

a detailed study of conditions for thermally dominated fragmentation), producing thus a flattening of the velocity spectrum. Note that Heitsch et al. (2008) find that outside the strictly thermally unstable regions, in particular at large scales, there is a regime of densities, temperatures, and sizes where cooling still dominates and can lead to fragmentation when an external (ram or gravitational) pressure is applied. Although our results can be physically explained, they differ from the better established observational reports (Stanimirović & Lazarian 2001, Miville-Deschênes 2003). Other observational works (Dickey et al. 2001, Dutta et al. 2009) however, present results consistent with a very shallow structure functions. More observational data as well as a detailed high resolution numerical study (see §4.2) are thus needed in order to characterize the velocity spectrum behavior in a thermally bistable gas.

The behavior of the spectra obtained for specific temperature ranges is consistent with the behavior reported by Kim & Ryu (2005) in two ways: when  $M$  is changed within a specific range and when a fixed value of  $M$  is considered and we look to different temperature intervals. The spectra we get are however much shallower than those shown in Kim & Ryu (2005). A quantitative analysis regarding the slopes is not possible because we do not have enough resolution to ensure that structures at the three temperature intervals can expand over two decades in scale. The fact that a flattening of the spectrum for lower temperatures is only present in turbulence dominated simulations is also expected because in low  $M$  simulations thermal instability can proceed with almost no disturbances, leading to a better segregated gas where unstable gas is present only in the thin interfaces between cold and warm gas (see Figure 2). In turbulence dominated simulations, on the other hand, colder gas tends to be dominated by small scale density structure (see Figure 2) and thermally unstable gas spread over larger regions.

## 4.2. Resolution Considerations

The main limitation of this work is the relatively low resolution we have used,  $512^3$ , which can affect our results in different ways. Numerical diffusivity has consequences on the thermal behavior of the simulations because it acts as a no controlled thermal conductivity. Field's (1965)



analysis shows that in the absence of thermal conductivity the linear growth rate of TI reaches its maximum value and becomes constant for small enough scales, while for a thermally conducting gas if the perturbation scale is reduced, the growth rate decreases to zero. The scale at which TI is suppressed by conduction  $\lambda_F$ , is known as the Field length (Begelman & McKee 1990). The effect of a small resolution is to impose a "numerical Field length" which suppress the development of TI at artificially large scales, creating broader boundaries between cool and warm gas and larger cold structures. This effect is more relevant at low Mach numbers, when the pure development of TI dominates the simulations. For 2-dimensional simulations with  $512^2$  grid points, Gazol et al. (2005) have verified that density perturbations of amplitude 2.5% and wavelength  $\lambda = 16$  pixels (3.1 pc) remain stationary (thus being the numerical Field length), while perturbations with  $\lambda = 4$  pixels (0.8 pc) are completely damped in times  $\sim 3$  Myr. They also explored the growth rate concluding that  $512^2$  is an acceptable resolution for capturing the linear growth, in the presence of realistic conductivity, of modes with sizes down to  $1/16$  the box size. For the nonlinear case, density perturbations with large amplitude velocity perturbations, the difference between the growth rates for  $N = 512^2$  and  $N = 1024^2$  is smaller than for the pure density perturbation case. On the other hand the minimum size in our simulations ( $\approx 0.2$ pc) is larger than the typical size of the cold structures generated by pure TI ( $\approx 0.1$ pc), thus our simulations probably overestimate the sizes of those cloudlets that are formed by the instability rather than by larger scale, coherent turbulent compressions, and certainly do not resolve their internal structure. As a consequence, improving the resolution could affect the results concerning density spectra at specific temperature ranges because the cold and unstable gas distribution could be modified.

In Figure 10 (*left*) we show  $P_\rho(k)$  for three simulations with  $M = 0.6$  and three different resolutions:  $256^3$ ,  $512^3$ , and  $1024^3$ . As expected due to the increased numerical diffusivity, for the low resolution simulation the inertial range is very short and worse defined than in the other cases. However, the slope of the three spectra is very similar: -0.61, -0.60, -0.63. In the *right* panel of the same figure  $P_\rho(k)$  is shown for  $M \approx 4.5$  ( $M = 4.35, 4.55$

and  $4.51$  for  $1024^3$ ,  $512^3$  and  $256^3$ , respectively). In that case the effect of resolution is more important, slopes we find are -0.19, -0.10 and -0.25 for  $1024^3$ ,  $512^3$  and  $256^3$ , respectively. Velocity spectra for the same sets of simulations are displayed in Figure 11. For  $M = 0.6$  (*left*) important differences can be appreciated between the  $256^3$  spectrum on one hand and the  $512^3$  and  $1024^3$  on the other. For the last two cases slopes are -1.16 and -1.23 at  $512^3$  and  $1024^3$ , respectively. The *right* panel shows  $P_v(k)$  for  $M \approx 4.5$ , the resulting slopes in this case are -2.13, -1.79, and -1.55 for  $1024^3$ ,  $512^3$  and  $256^3$ , respectively. As for the density power spectrum, at larger  $M$  values the effect of resolution is more important but the fact that we obtain an even steeper spectrum for the large resolution simulation suggest that the steepening of the velocity spectrum as  $M$  increases is not a numerical artifact. For the low resolution simulation spectra have been computed by averaging over several snapshots at the same time interval as the one stated in Table 1 for the  $M = 0.6$  simulation, while for the high resolution case we used few snapshots around 4.5 turbulent crossing times. The resolution study on density spectra showed a better convergence than that on velocity spectra. It is due to the fact that, on density fields, there is the additional constraint of mass conservation inside our computational box, irrespectively of the numerical resolution.

## 5. Summary and Conclusions

In this paper we investigated the behavior of the density power spectrum of forced, thermally bistable flows in physical conditions similar to those of the atomic interstellar gas and with different Mach numbers. Our main results can be summarized as follows:

1. For thermally bistable flows, the density spectrum flattens as the Mach number is increased. This is the same behavior as the one previously reported for isothermal turbulence (Kim & Ryu 2005), but in the present case the spectral slopes are shallower. We interpret this fact and the behavior with  $M$  as a consequence of a combined effect of the presence of strong density fluctuations produced by TI and turbulence with the fact that the larger is  $M$ , the weaker are pressure forces in diffuse gas produced by the

interaction of turbulence and TI.

2. The velocity power spectrum exhibits an opposite behavior, i.e. it becomes steeper as the Mach number increases. The spectral indexes go from values much lower than the Kolmogorov slope for small  $M$  to a value larger than it for the larger Mach number. We hypothesize that the flattening of the spectrum for low  $M$  could be due to the increased relevance of the velocities generated by the development of TI, but a detailed analysis of the velocity power spectrum for thermally bistable flows is needed.

3. Comparison with observations show that the spectral slopes we obtain are consistent with some of the results on the three dimensional atomic power spectrum. If we use predictions of the VCA method to compare with observational slopes of the spatial power spectrum (which contains information about the three dimensional density as well as about the three dimensional velocity field), then our results are also consistent with observations.

4. The density power spectrum at specific temperature ranges shows a behavior that seems to be consistent with the first point of this summary but an analysis with much larger numerical resolution is still needed.

5. Resolution effects, in particular for large  $M$  simulations, can probably change the spectral slopes but the behaviors we describe and summarize in previous points are not modified by these effects.

In conclusion, the presence of TI does significantly affect the statistics of turbulence. Different turbulence conditions, in particular different Mach numbers, can lead to considerably different slopes of the density and the velocity power spectrum of the atomic interstellar gas. Given the fact that the amount of available kinetic energy can change from one place to another, differences in observational results concerning the density power spectrum could be, at least partially, be explained by this effect. Note however that in order to relate the density power spectrum with the Mach number observational studies must clearly separate contributions from the density distribution and contributions from the velocity field.

We would like to acknowledge an anonymous referee for suggestions to improve this work. The

work of A. G. was partially supported by UNAM-DGAPA grant IN111006-3. The work of J.K. was supported by the National Research Foundation of Korea through 2009-0062863 (ARCSEC). Numerical simulations were performed at the cluster Platform 4000 (KanBalam) at DGSCA, UNAM and at the Linux Cluster for Astronomical Computations of KASI-ARCSEC.

## REFERENCES

- Armstrong, J. W., Rickett, B. J., & Spangler, S. R. 1995, *ApJ*, 443, 209
- Bensch, F., Stutzki, J. and Ossenkopf, V. 2001, *A&A*, 366, 636
- Begelman, M. C., & McKee, C. F. 1990, *ApJ*, 358, 375
- Boulanger, F., & Viallefond, F. 1992, *A&A*, 266, 37
- Brunt, C. M., Federrath, C. & Price, D.J. 2010, *MNRAS*, 403, 1507
- Brunt, C. M., Heyer, M. H., & Mac Low, M.-M. 2009, *A&A*, 504, 883
- Crovisier, J., & Dickey, J. M. 1983, *A&A*, 122, 282
- Deshpande, A. A., Dwarakanath, K. S., & Goss, W. M. 2000, *ApJ*, 543, 227
- Dickey, J. M., McClure-Griffiths, N. M., Stanimirović, S., Gaensler, B. M., & Green A. J. 2001, *ApJ*, 561, 264
- Dutta, P., Begum, A., Bharadwaj, S., & Chengar, J. N. 2009 *MNRAS*, 398, 887
- Elmegreen, B. G., Kim, S., & Staveley-Smith, L. 2001 *ApJ*, 58, 749
- Elmegreen, B. G., Scalo J. 2004, *ARA&A*, 42, 211
- Federrath, C., Klessen, R. S., & Schmidt, W. 2008, *ApJ*, 688, L79
- Federrath, C., Klessen, R. S., & Schmidt, W. 2009, *ApJ*, 692, 364
- Federrath, C., Roman-Duval, J., Klessen, R. S., Schmidt, W., & Mac Low, M.-M. 2010, *A&A*, 512, 81

- Field, G. B. 1965, *ApJ*, 142, 531
- Gazol, A., Vázquez-Semadeni, E., & Kim, J. 2005 *ApJ*, 630, 911
- Green, D. A. 1993, *MNRAS*, 262, 327
- Harten, A. 1983, *J. Comput. Phys.*, 49, 357
- Heitsch, F., Hartmann, L. & Burkert A. 2008, *ApJ*, 683, 786
- Hennebelle, P., Mac Low, M. -M., & Vazquez-Semadeni, E. in *Structure Formation in Astrophysics*, edited by Gilles Chabrier, Cambridge University Press, Cambridge, UK, 2009, p.205
- Hennebelle, P. & Audit, E. 2007, *A&A*, 465, 431
- Hennebelle, P., & Péroult, M. 1999, *A&A*, 351, 309
- Hodge, J. A., & Deshpande, A. A. 2006, *ApJ*, 646, 232
- Klessen, R. S. 2000, *ApJ*, 535, 869
- Kim, J., & Ryu, D. 2005, *ApJ*, 630, L45
- Kim, J., Ryu, D., Jones, T. W., & Hong, S. S. 1999, *ApJ*, 514, 506
- Kitsionas, S., Klessen, R. S., Federrath, C., Schmidt, W., Price, D., Dursi, J., Gritschneider, M., Walch, S., Piontek, R., Kim, J., Jappsen, A. -K., Cieliegl, P., Mac Low, M. -M. 2009, *A&A*, 508, 549
- Kritsuk, A., & Norman, M. L. 2002, *ApJ*, 569, L127
- Kritsuk, A., Norman, M. L., Padoan, P., & Wagner, R. 2007, *ApJ*, 665, 416
- Kowal, G., Lazarian, A., & Beresnyak, A. 2007, *ApJ*, 658, 423
- Lazarian, A. & Pogosyan, D. 2000, *ApJ*, 537, 720
- Li, Y., Klessen R. S., & Mac Low, M. M. 2003, *ApJ*, 592, 975
- Lighthill, M. J. 1955, in *IAU Symp. 2, Gas Dynamics of Cosmic Clouds* (Amsterdam: North Holland), 121
- Mac Low, M.-M. 1999, *ApJ* 524, 169
- Mac Low, M.-M., & Klessen, R. S. 2004, *Reviews of Modern Physics*, 76, 125
- Mac Low, M.-M., & Ossenkopf, V. 2000, *A&A*, 353, 339
- Miville-Deschênes, M.-A., Joncas, G., Falgarone, E., & Boulanger, F. 2003, *A&A*, 411, 109
- Nordlund, Å., & Padoan, P. 1999, in *Interstellar Turbulence*, eds. J. Franco and A. Carramiñana (Cambridge: Cambridge University Press), p. 218
- Padoan, P., Juvela, M., Kritsuk, A., & Norman, M. L. 2006, *ApJ*, 653, L125
- Passot, T., & Vazquez-Semadeni, E. 1998, *Phys. Rev. E* 1999, 58, 4501
- Petric, A. O., & Rupen, M. P. 2007, *AJ*, 134, 1952
- Piontek, R. A., & Ostriker, E. C. 2004, *ApJ*, 601, 905
- Roe, P. L. 1981, *J. Comput. Phys.*, 49, 357
- Rownd, B. K., Dickey, J. M., & Helou, G. 1994, *AJ*, 108, 1638
- Sachiev, A. I., & Woyczynski, W. A. 1996, *SIAM J. Appl. Math.*, 56, 1008
- Sánchez-Salcedo, F. J., Vázquez-Semadeni, E., & Gazol, A. 2002, *ApJ*, 577, 768
- Scalo, J., & Elmegreen, B. G. 2004, *ARA&A*, 42, 275
- Schmidt, W., Federrath, C., Hupp, M., Kern, S., & Niemeyer, J. C 2009, *A&A*, 494, 127
- Stanimirović, S., & Lazarian, A. 2001, *ApJ*, 551, L53
- Stanimirović, S., Stavely-Smith, L., Dickey, J. M., Sault, R. J., Snowden, S. L. 1999, *MNRAS*, 302, 417
- Stutzki, J., Bensch, F., Heithausen, A., Ossenkopf, V. & Zielinsky, M. 1998, *A&A*, 336, 697
- Tamburro, D., Rix, H. W., Leroy, A. K., MacLow, M. M., Walter, F., Kennicutt, R. C., Brinks, E., & de Blok, W. J. G. 2009 *AJ*, 137, 4424

Wolfire, M. G., Hollenbach, D., McKee, C. F., Tielens, A. G. G. M. & Bakes, E. L. O. 1995, *ApJ*, 443, 152

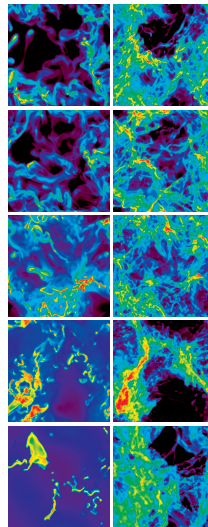


Fig. 1.— *Left column* : Color images of the density distribution in a two-dimensional slice for each simulation. All the panels in this column have been done with the same color scale ranging from  $10^{-1.5}\text{cm}^{-3}$  to  $10^{1.5}\text{cm}^{-3}$ . *Right column* : Column density distribution for each simulation. All the panels in this column have been done with the same color scale ranging from  $10^{-1.5}\text{cm}^{-3}$  and  $10^{1.5}\text{cm}^{-3}$ . On both sides, the value of  $M$  decreases from top to bottom, from 4.5 to 0.2. Redder colors indicate denser gas. For each simulation the images has been done at the last time considered when computing averaged spectra (see Table 1).

This 2-column preprint was prepared with the AAS L<sup>A</sup>T<sub>E</sub>X macros v5.2.

TABLE 1  
TIME PARAMETERS

$M$	$t_f^a$	$\Delta t^b$	$N_{\text{outputs}}^c$	$t_{f0}^d$
0.2	6.0	2.0-6.0	21	30
0.6	10.2	3.0-9.0	21	15
1.3	9.0	2.8-8.3	24	7
4.0	16.0	8.0-16.0	21	4
4.5	18.0	9.0-18.0	21	4

<sup>a</sup>End time of each simulation in units of the turbulent crossing time

<sup>b</sup>Time interval over which time averaged spectra are computed

<sup>c</sup>Number of outputs used for temporal averages

<sup>d</sup>End time of each simulation in code time units

TABLE 2  
SPECTRAL INDEX

$M$	$P_\rho$	$P_\Sigma$	$P_v$	$P_{\rho^{1/2}v}$	$P_{\rho^{1/3}v}$	$P_{w\rho}^a$	$P_{u\rho}^b$	$P_{c\rho}^c$
0.2	-0.84	-1.64	-1.08	-0.77	-0.89	-0.77	-0.79	-0.84
0.6	-0.60	-1.52	-1.16	-0.77	-0.94	-0.57	-0.55	-0.59
1.3	-0.20	-1.14	-1.51	-0.80	-1.11	-0.51	-0.27	-0.12
4.0	-0.15	-1.11	-1.78	-0.85	-1.19	-0.19	-0.24	0.04
4.5	-0.10	-1.19	-1.79	-0.84	-1.18	-0.18	-0.19	0.09

<sup>a</sup>Density power spectrum for gas with  $T > 6110\text{K}$

<sup>b</sup>Density power spectrum for gas with  $313\text{K} < T < 6110\text{K}$

<sup>c</sup>Density power spectrum for gas with  $T < 313\text{K}$

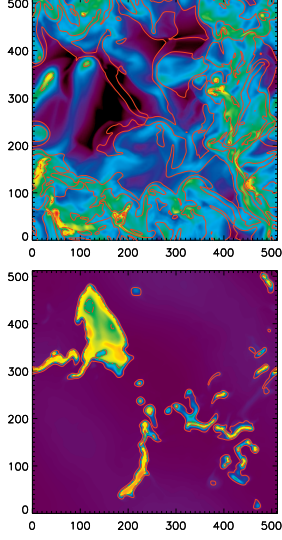


Fig. 2.— Same density slices as in figure 1 for  $M = 4.5$  (top) and  $M = 0.2$  (bottom) but with different color scales. For  $M = 4.5$  color scale ranges from  $10^{-2.5}\text{cm}^{-3}$  to  $10^2\text{cm}^{-3}$  while for  $M_{rms} = 0.2$  it goes from  $10^{-1.2}\text{cm}^{-3}$  to  $10^{1.5}\text{cm}^{-3}$ . In both panels, *solid line* and *dashed line* contours are placed at 6110K and 313K, respectively.

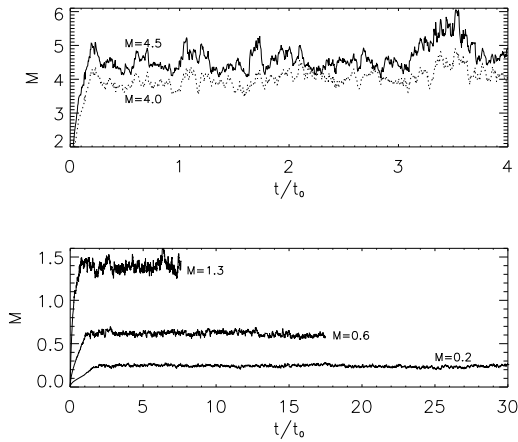


Fig. 3.—  $M_{rms}$  as a function of time for the five simulations discussed in §3. The x-axis is code time units  $t_0$ .

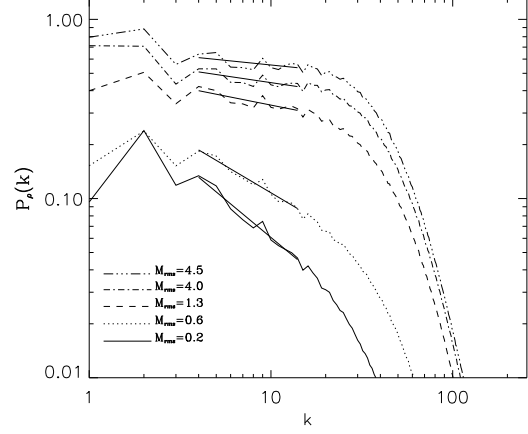


Fig. 4.— Density power spectra  $P_\rho$  for simulations with different  $M$ . Solid lines represent least-squares fits over the range  $4 \leq k \leq 14$ .

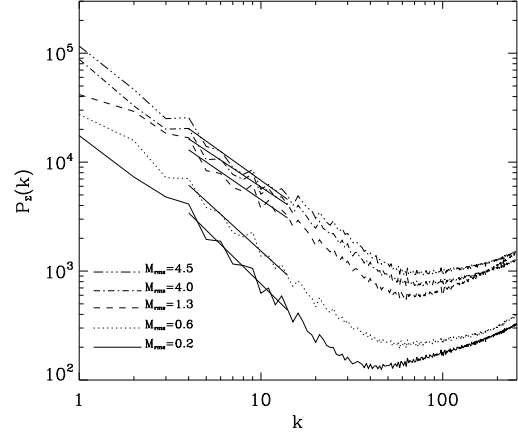


Fig. 5.— Column density power spectra  $P_\Sigma$  for simulations with different  $M$ . The two dimensional density distribution is obtained by projecting the full three-dimensional density field on the  $z$  direction. Solid lines represent least-squares fits over the range  $4 \leq k \leq 14$ .

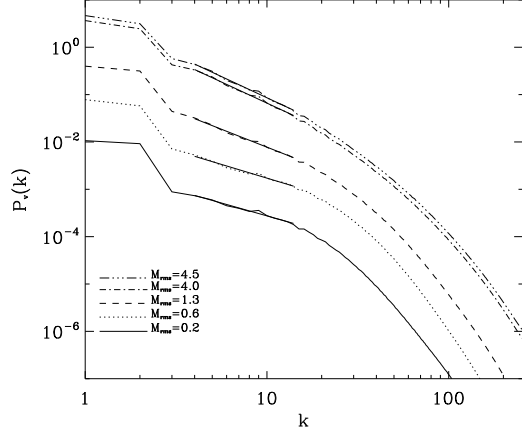


Fig. 6.— Velocity power spectra  $P_v$  for simulations with different  $M$ . Solid lines represent least-squares fits over the range  $4 \leq k \leq 14$ .

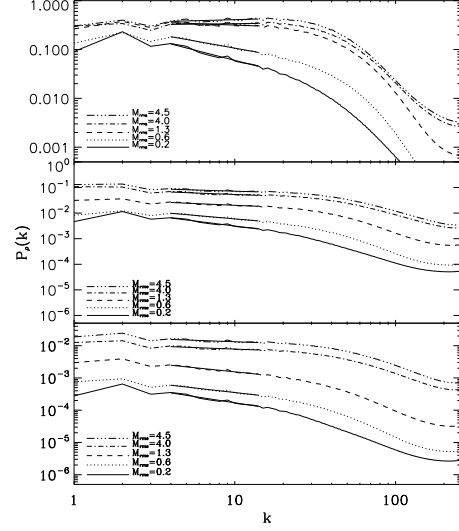


Fig. 8.— Density power spectra for gas at different temperature ranges resulting from simulations with different  $M$ . In the three panels solid lines represent least-squares fits over the range  $4 \leq k \leq 14$ . *Top* : Density power spectra for cold gas ( $T \leq 313\text{K}$ ). *Middle* : Density power spectra for thermally unstable gas ( $313\text{K} < T < 6110\text{K}$ ). *Bottom* : Density power spectra for warm gas ( $T \geq 6110\text{K}$ ).

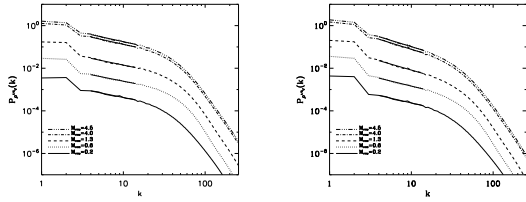


Fig. 7.— Power spectra of  $\rho^{1/2}v$ ,  $P_{\rho^{1/2}v}$  (left) and  $\rho^{1/3}v$ ,  $P_{\rho^{1/3}v}$  (right) for simulations with different  $M$ . Solid lines represent least-squares fits over the range  $4 \leq k \leq 14$ .

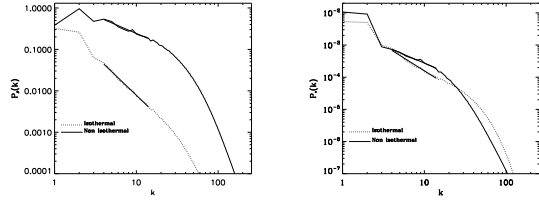


Fig. 9.— Density (left) and velocity (right) power spectra for a thermally unstable simulation (solid line) and an isothermal one (dotted line), both at  $M = 0.2$ . Solid lines represent least-squares fits over the range  $4 \leq k \leq 14$ .

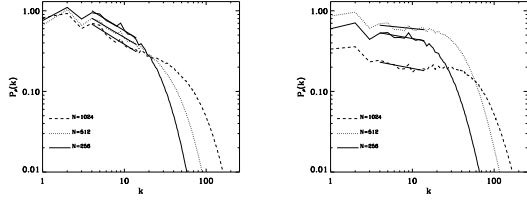


Fig. 10.— Density power spectra  $P_\rho$  for simulations with  $M = 0.6$  (*left*) and  $M = 4.5$  (*right*), and different resolutions. Solid lines represent least-squares fits over the range  $4 \leq k \leq 14$ .

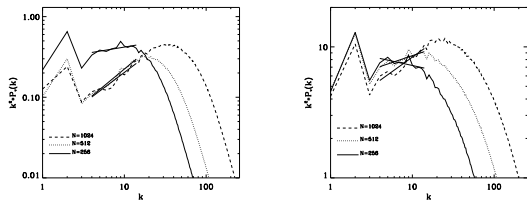


Fig. 11.— Compensated velocity power spectra  $k^2 P_v$  for simulations with  $M = 0.6$  (*left*) and  $M = 4.5$  (*right*), and different resolutions. Solid lines represent least-squares fits over the range  $4 \leq k \leq 14$ .